

J/ψ Production and Nuclear Effects for $d + Au$ and $p + p$ Collisions at $\sqrt{s_{NN}} = 200$ GeV

S.S. Adler,⁵ S. Afanasiev,²⁰ C. Aidala,¹⁰ N.N. Ajitanand,⁴⁴ Y. Akiba,^{21,40} A. Al-Jamel,³⁵ J. Alexander,⁴⁴ K. Aoki,²⁵ L. Aphecetche,⁴⁶ R. Armendariz,³⁵ S.H. Aronson,⁵ E.T. Atomssa,²⁶ R. Auerbeck,⁴⁵ T.C. Awes,³⁶ V. Babintsev,¹⁷ A. Baldisseri,¹¹ K.N. Barish,⁶ P.D. Barnes,²⁸ B. Bassalleck,³⁴ S. Bathe,^{6,31} S. Batsouli,¹⁰ V. Baublil,³⁹ F. Bauer,⁶ A. Bazilevsky,^{5,41} S. Belikov,^{19,17} M.T. Bjornrdal,¹⁰ J.G. Boissevain,²⁸ H. Borel,¹¹ M.L. Brooks,²⁸ D.S. Brown,³⁵ N. Bruner,³⁴ D. Bucher,³¹ H. Buesching,^{5,31} V. Bumazhnov,¹⁷ G. Bunce,^{5,41} J.M. Burward-Hoy,^{28,27} S. Butsyk,⁴⁵ X. Camard,⁴⁶ P. Chand,⁴ W.C. Chang,² S. Chernichenko,¹⁷ C.Y. Chi,¹⁰ J. Chiba,²¹ M. Chiu,¹⁰ I.J. Choi,⁵³ R.K. Choudhury,⁴ T. Chujo,⁵ V. Cianciolo,³⁶ Y. Cobigo,¹¹ B.A. Cole,¹⁰ M.P. Comets,³⁷ P. Constantin,¹⁹ M. Csanád,¹³ T. Csörgő,²² J.P. Cussonneau,⁴⁶ D. d'Enterria,¹⁰ K. Das,¹⁴ G. David,⁵ F. Deák,¹³ H. Delagrangé,⁴⁶ A. Denisov,¹⁷ A. Deshpande,⁴¹ E.J. Desmond,⁵ A. Devismes,⁴⁵ O. Dietzsch,⁴² J.L. Drachenberg,¹ O. Drapier,²⁶ A. Drees,⁴⁵ A. Durum,¹⁷ D. Dutta,⁴ V. Dzhordzhadze,⁴⁷ Y.V. Efremenko,³⁶ H. En'yo,^{40,41} B. Espagnon,³⁷ S. Esumi,⁴⁹ D.E. Fields,^{34,41} C. Finck,⁴⁶ F. Fleuret,²⁶ S.L. Fokin,²⁴ B.D. Fox,⁴¹ Z. Fraenkel,⁵² J.E. Frantz,¹⁰ A. Franz,⁵ A.D. Frawley,¹⁴ Y. Fukao,^{25,40,41} S.-Y. Fung,⁶ S. Gadrat,²⁹ M. Germain,⁴⁶ A. Glenn,⁴⁷ M. Gonin,²⁶ J. Gosset,¹¹ Y. Goto,^{40,41} R. Granier de Cassagnac,²⁶ N. Grau,¹⁹ S.V. Greene,⁵⁰ M. Grosse Perdekamp,^{18,41} H.-Å. Gustafsson,³⁰ T. Hachiya,¹⁶ J.S. Haggerty,⁵ H. Hamagaki,⁸ A.G. Hansen,²⁸ E.P. Hartouni,²⁷ M. Harvey,⁵ K. Hasuko,⁴⁰ R. Hayano,⁸ X. He,¹⁵ M. Heffner,²⁷ T.K. Hemmick,⁴⁵ J.M. Heuser,⁴⁰ P. Hidas,²² H. Hiejima,¹⁸ J.C. Hill,¹⁹ R. Hobbs,³⁴ W. Holzmann,⁴⁴ K. Homma,¹⁶ B. Hong,²³ A. Hoover,³⁵ T. Horaguchi,^{40,41,48} T. Ichihara,^{40,41} V.V. Ikonnikov,²⁴ K. Imai,^{25,40} M. Inaba,⁴⁹ M. Inuzuka,⁸ D. Isenhower,¹ L. Isenhower,¹ M. Ishihara,⁴⁰ M. Issah,⁴⁴ A. Isupov,²⁰ B.V. Jacak,⁴⁵ J. Jia,⁴⁵ O. Jinnouchi,^{40,41} B.M. Johnson,⁵ S.C. Johnson,²⁷ K.S. Joo,³² D. Jouan,³⁷ F. Kajihara,⁸ S. Kametani,^{8,51} N. Kamihara,^{40,48} M. Kaneta,⁴¹ J.H. Kang,⁵³ K. Katou,⁵¹ T. Kawabata,⁸ A.V. Kazantsev,²⁴ S. Kelly,^{9,10} B. Khachaturov,⁵² A. Khanzadeev,³⁹ J. Kikuchi,⁵¹ D.J. Kim,⁵³ E. Kim,⁴³ G.-B. Kim,²⁶ H.J. Kim,⁵³ E. Kinney,⁹ A. Kiss,¹³ E. Kistenev,⁵ A. Kiyomichi,⁴⁰ C. Klein-Boesing,³¹ H. Kobayashi,⁴¹ L. Kochenda,³⁹ V. Kochetkov,¹⁷ R. Kohara,¹⁶ B. Komkov,³⁹ M. Konno,⁴⁹ D. Kotchetkov,⁶ A. Kozlov,⁵² P.J. Kroon,⁵ C.H. Kuberg,^{1,*} G.J. Kunde,²⁸ K. Kurita,⁴⁰ M.J. Kweon,²³ Y. Kwon,⁵³ G.S. Kyle,³⁵ R. Lacey,⁴⁴ J.G. Lajoie,¹⁹ Y. Le Bornec,³⁷ A. Lebedev,^{19,24} S. Leckey,⁴⁵ D.M. Lee,²⁸ M.J. Leitch,²⁸ M.A.L. Leite,⁴² X.H. Li,⁶ H. Lim,⁴³ A. Litvinenko,²⁰ M.X. Liu,²⁸ C.F. Maguire,⁵⁰ Y.I. Makdisi,⁵ A. Malakhov,²⁰ V.I. Manko,²⁴ Y. Mao,^{38,40} G. Martinez,⁴⁶ H. Masui,⁴⁹ F. Matathias,⁴⁵ T. Matsumoto,^{8,51} M.C. McCain,¹ P.L. McGaughey,²⁸ Y. Miake,⁴⁹ T.E. Miller,⁵⁰ A. Milov,⁴⁵ S. Mioduszewski,⁵ G.C. Mishra,¹⁵ J.T. Mitchell,⁵ A.K. Mohanty,⁴ D.P. Morrison,⁵ J.M. Moss,²⁸ D. Mukhopadhyay,⁵² M. Muniruzzaman,⁶ S. Nagamiya,²¹ J.L. Nagle,^{9,10} T. Nakamura,¹⁶ J. Newby,⁴⁷ A.S. Nyanin,²⁴ J. Nystrand,³⁰ E. O'Brien,⁵ C.A. Ogilvie,¹⁹ H. Ohnishi,⁴⁰ I.D. Ojha,^{3,50} H. Okada,^{25,40} K. Okada,^{40,41} A. Oskarsson,³⁰ I. Otterlund,³⁰ K. Oyama,⁸ K. Ozawa,⁸ D. Pal,⁵² A.P.T. Palounek,²⁸ V. Pantuev,⁴⁵ V. Papavassiliou,³⁵ J. Park,⁴³ W.J. Park,²³ S.F. Pate,³⁵ H. Pei,¹⁹ V. Penev,²⁰ J.-C. Peng,¹⁸ H. Pereira,¹¹ V. Peresedov,²⁰ A. Pierson,³⁴ C. Pinkenburg,⁵ R.P. Pisani,⁵ M.L. Purschke,⁵ A.K. Purwar,⁴⁵ J.M. Qualls,¹ J. Rak,¹⁹ I. Ravinovich,⁵² K.F. Read,^{36,47} M. Reuter,⁴⁵ K. Reygers,³¹ V. Riabov,³⁹ Y. Riabov,³⁹ G. Roche,²⁹ A. Romana,^{26,*} M. Rosati,¹⁹ S.S.E. Rosendahl,³⁰ P. Rosnet,²⁹ V.L. Rykov,⁴⁰ S.S. Ryu,⁵³ N. Saito,^{25,40,41} T. Sakaguchi,^{8,51} S. Sakai,⁴⁹ V. Samsonov,³⁹ L. Sanfratello,³⁴ R. Santo,³¹ H.D. Sato,^{25,40} S. Sato,^{5,49} S. Sawada,²¹ Y. Schutz,⁴⁶ V. Semenov,¹⁷ R. Seto,⁶ T.K. Shea,⁵ I. Shein,¹⁷ T.-A. Shibata,^{40,48} K. Shigaki,¹⁶ M. Shimomura,⁴⁹ A. Sickles,⁴⁵ C.L. Silva,⁴² D. Silvermyr,²⁸ K.S. Sim,²³ A. Soldatov,¹⁷ R.A. Soltz,²⁷ W.E. Sondheim,²⁸ S.P. Sorensen,⁴⁷ I.V. Sourikova,⁵ F. Staley,¹¹ P.W. Stankus,³⁶ E. Stenlund,³⁰ M. Stepanov,³⁵ A. Ster,²² S.P. Stoll,⁵ T. Sugitate,¹⁶ J.P. Sullivan,²⁸ S. Takagi,⁴⁹ E.M. Takagui,⁴² A. Taketani,^{40,41} K.H. Tanaka,²¹ Y. Tanaka,³³ K. Tanida,⁴⁰ M.J. Tannenbaum,⁵ A. Taranenko,⁴⁴ P. Tarján,¹² T.L. Thomas,³⁴ M. Togawa,^{25,40} J. Tojo,⁴⁰ H. Torii,^{25,41} R.S. Towell,¹ V.-N. Tram,²⁶ I. Tserruya,⁵² Y. Tsuchimoto,¹⁶ H. Tydesjö,³⁰ N. Tyurin,¹⁷ T.J. Uam,³² H.W. van Hecke,²⁸ J. Velkovska,⁵ M. Velkovsky,⁴⁵ V. Veszprémi,¹² A.A. Vinogradov,²⁴ M.A. Volkov,²⁴ E. Vznuzdaev,³⁹ X.R. Wang,¹⁵ Y. Watanabe,^{40,41} S.N. White,⁵ N. Willis,³⁷ F.K. Wohn,¹⁹ C.L. Woody,⁵ W. Xie,⁶ A. Yanovich,¹⁷ S. Yokkaichi,^{40,41} G.R. Young,³⁶ I.E. Yushmanov,²⁴ W.A. Zajc,^{10,†} C. Zhang,¹⁰ S. Zhou,⁷ J. Zimányi,²² L. Zolin,²⁰ and X. Zong¹⁹

(PHENIX Collaboration)

¹Abilene Christian University, Abilene, TX 79699, USA²Institute of Physics, Academia Sinica, Taipei 11529, Taiwan³Department of Physics, Banaras Hindu University, Varanasi 221005, India⁴Bhabha Atomic Research Centre, Bombay 400 085, India

- ⁵Brookhaven National Laboratory, Upton, NY 11973-5000, USA
⁶University of California - Riverside, Riverside, CA 92521, USA
⁷China Institute of Atomic Energy (CIAE), Beijing, People's Republic of China
⁸Center for Nuclear Study, Graduate School of Science, University of Tokyo, 7-3-1 Hongo, Bunkyo, Tokyo 113-0033, Japan
⁹University of Colorado, Boulder, CO 80309, USA
¹⁰Columbia University, New York, NY 10027 and Nevis Laboratories, Irvington, NY 10533, USA
¹¹Dapnia, CEA Saclay, F-91191, Gif-sur-Yvette, France
¹²Debrecen University, H-4010 Debrecen, Egyetem tér 1, Hungary
¹³ELTE, Eötvös Loránd University, H - 1117 Budapest, Pázmány P. s. 1/A, Hungary
¹⁴Florida State University, Tallahassee, FL 32306, USA
¹⁵Georgia State University, Atlanta, GA 30303, USA
¹⁶Hiroshima University, Kagamiyama, Higashi-Hiroshima 739-8526, Japan
¹⁷IHEP Protvino, State Research Center of Russian Federation, Institute for High Energy Physics, Protvino, 142281, Russia
¹⁸University of Illinois at Urbana-Champaign, Urbana, IL 61801, USA
¹⁹Iowa State University, Ames, IA 50011, USA
²⁰Joint Institute for Nuclear Research, 141980 Dubna, Moscow Region, Russia
²¹KEK, High Energy Accelerator Research Organization, Tsukuba, Ibaraki 305-0801, Japan
²²KFKI Research Institute for Particle and Nuclear Physics of the Hungarian Academy of Sciences (MTA KFKI RMKI), H-1525 Budapest 114, POBox 49, Budapest, Hungary
²³Korea University, Seoul, 136-701, Korea
²⁴Russian Research Center "Kurchatov Institute", Moscow, Russia
²⁵Kyoto University, Kyoto 606-8502, Japan
²⁶Laboratoire Leprince-Ringuet, Ecole Polytechnique, CNRS-IN2P3, Route de Saclay, F-91128, Palaiseau, France
²⁷Lawrence Livermore National Laboratory, Livermore, CA 94550, USA
²⁸Los Alamos National Laboratory, Los Alamos, NM 87545, USA
²⁹LPC, Université Blaise Pascal, CNRS-IN2P3, Clermont-Fd, 63177 Aubiere Cedex, France
³⁰Department of Physics, Lund University, Box 118, SE-221 00 Lund, Sweden
³¹Institut für Kernphysik, University of Muenster, D-48149 Muenster, Germany
³²Myongji University, Yongin, Kyonggido 449-728, Korea
³³Nagasaki Institute of Applied Science, Nagasaki-shi, Nagasaki 851-0193, Japan
³⁴University of New Mexico, Albuquerque, NM 87131, USA
³⁵New Mexico State University, Las Cruces, NM 88003, USA
³⁶Oak Ridge National Laboratory, Oak Ridge, TN 37831, USA
³⁷IPN-Orsay, Université Paris Sud, CNRS-IN2P3, BP1, F-91406, Orsay, France
³⁸Peking University, Beijing, People's Republic of China
³⁹PNPI, Petersburg Nuclear Physics Institute, Gatchina, Leningrad region, 188300, Russia
⁴⁰RIKEN (The Institute of Physical and Chemical Research), Wako, Saitama 351-0198, JAPAN
⁴¹RIKEN BNL Research Center, Brookhaven National Laboratory, Upton, NY 11973-5000, USA
⁴²Universidade de São Paulo, Instituto de Física, Caixa Postal 66318, São Paulo CEP05315-970, Brazil
⁴³System Electronics Laboratory, Seoul National University, Seoul, South Korea
⁴⁴Chemistry Department, Stony Brook University, Stony Brook, SUNY, NY 11794-3400, USA
⁴⁵Department of Physics and Astronomy, Stony Brook University, SUNY, Stony Brook, NY 11794, USA
⁴⁶SUBATECH (Ecole des Mines de Nantes, CNRS-IN2P3, Université de Nantes) BP 20722 - 44307, Nantes, France
⁴⁷University of Tennessee, Knoxville, TN 37996, USA
⁴⁸Department of Physics, Tokyo Institute of Technology, Oh-okayama, Meguro, Tokyo 152-8551, Japan
⁴⁹Institute of Physics, University of Tsukuba, Tsukuba, Ibaraki 305, Japan
⁵⁰Vanderbilt University, Nashville, TN 37235, USA
⁵¹Waseda University, Advanced Research Institute for Science and Engineering, 17 Kikui-cho, Shinjuku-ku, Tokyo 162-0044, Japan
⁵²Weizmann Institute, Rehovot 76100, Israel
⁵³Yonsei University, IPAP, Seoul 120-749, Korea

(Dated: October 17, 2018)

J/ψ production in $d + Au$ and $p + p$ collisions at $\sqrt{s_{NN}} = 200$ GeV has been measured by the PHENIX experiment at rapidities $-2.2 < y < +2.4$. The cross sections and nuclear dependence of J/ψ production versus rapidity, transverse momentum, and centrality are obtained and compared to lower energy $p + A$ results and to theoretical models. The observed nuclear dependence in $d + Au$ collisions is found to be modest, suggesting that the absorption in the final state is weak and the shadowing of the gluon distributions is small and consistent with Dokshitzer-Gribov-Lipatov-Altarelli-Parisi-based parameterizations that fit deep-inelastic scattering and Drell-Yan data at lower energies.

J/ψ production in hadron collisions, since it proceeds predominantly through diagrams involving gluons (e.g. gluon fusion) [1], is a sensitive probe of the gluon structure function in the nucleon and its modification in nuclei. It is also a leading signal for the creation of hot-dense matter in heavy-ion collisions [2]. Shadowing of partons (quarks or gluons) in nuclei is a depletion of their population at small momentum fraction of the nucleon, x , compared to that in a free nucleon, with a corresponding enhancement at moderate x (anti-shadowing). In $\sqrt{s_{NN}} = 200$ GeV deuteron-gold ($d+Au$) collisions at the Relativistic Heavy Ion Collider (RHIC), for positive (deuteron direction) rapidities, gluons are probed that lie well into the shadowing region with momentum fractions in Au , $x_2 \sim 3 \times 10^{-3}$. Models of gluon shadowing predict suppressions of J/ψ production in nuclei that differ by as much as a factor of three [3, 4, 5]. Recent theoretical developments, e.g. the Color Glass Condensate model [6], suggest that at very low x non-linear gluon saturation effects become important and cause substantial modifications of the gluon densities.

The connection of the observed J/ψ suppression to the modified gluon distribution in nuclei can be clouded by the absorption of the final-state $c\bar{c}$ [7] which depends on the poorly known production mechanism [1] and by the energy loss of the initial-state gluon - although the latter is thought to be small at RHIC energies [5]. This connection is also distorted by the fact that approximately a third of the J/ψ 's come from decays of higher-mass resonances [8].

Here we present measurements made by the PHENIX experiment at RHIC for the production of J/ψ 's in $\sqrt{s_{NN}} = 200$ GeV $d+Au$ and proton-proton ($p+p$) collisions. These data provide the first measurement of the nuclear dependence of J/ψ production at this energy, a much higher energy than previous $p+A$ measurements from fixed-target experiments at $\sqrt{s_{NN}} \lesssim 40$ GeV [9, 10, 11, 12, 13]. Although our measurements are for $d+A$, the nuclear effects on the J/ψ in deuterium were found to be small at lower energies [14]. Besides the shadowing region at small x , these data also probe larger gluon momentum fractions (at negative rapidity) nearer the rest frame of the residual nucleus. Finally, these measurements also serve as a baseline for the upcoming results from the high-luminosity $Au+Au$ and $Cu+Cu$ runs and must be understood in order to look for effects beyond what is expected from cold nuclear matter.

The measurements described here are similar to earlier ones with PHENIX [15] for $p+p$ [16] and $Au+Au$ [17] collisions, but with a second muon spectrometer added and higher luminosity. The two muon spectrometers are especially valuable for asymmetric collisions such as $d+Au$ where simultaneous measurements at positive ($1.2 < y < 2.4$) and negative ($-2.2 < y < -1.2$) rapidities, along with central ($|y| \leq 0.35$) rapidity from e^+e^- ,

are then available. Electrons in the central arms are identified by matching charged particle tracks to clusters in an electromagnetic calorimeter (EMC) and to rings in a ring imaging Čerenkov (RICH) detector. Muons are identified by their detection in Iarocci tubes after their penetration through 8 to 11 interaction lengths of copper and steel absorber.

The data used in this analysis were recorded in 2003 using a trigger that required hits in each of the two beam-beam counters located at negative and positive rapidity ($3 < |\eta| < 3.9$). In addition, for the di-muons at least two tracks in the muon identifier of appropriate absorber depth were required, while for the di-electrons a one-track trigger with a signal above threshold in the EMC with a matching hit in the RICH was required. After quality and vertex cuts, the samples for the three arms correspond to integrated luminosities from 180 to 250 nb^{-1} ($p+p$) and 1.4 to 1.7 nb^{-1} ($d+Au$).

For the di-muons the J/ψ yield is obtained after subtraction of the combinatoric background using like-sign muon pairs ($2\sqrt{N_{++}N_{--}}$) and by fitting the resulting mass peak with a Gaussian plus an exponential to represent the small remaining continuum background underneath the peak. A variety of continuum shapes were checked for each fit in order to establish the uncertainty due to the low-statistics background. For the di-electrons the combinatoric background was subtracted using the sum of like-sign pairs and the J/ψ yield was taken as all remaining events in the mass range 2.6 to 3.6 GeV/c^2 . A total ($p+p$ plus $d+Au$) of about 2100 and 500 J/ψ 's were obtained in the $\mu\mu$ and ee channels, respectively.

The differential cross sections are calculated as,

$$B_{ll} \frac{d\sigma_{J/\psi}}{dy} = \frac{N_{J/\psi}}{A \epsilon_{rec} \epsilon_{trig} \epsilon_{J/\psi}^{BBC} (N_{evt} / (\sigma_{MB}^{tot} \cdot \epsilon_{MB}^{BBC}))} \frac{1}{\Delta y} \quad (1)$$

and the nuclear modification factor, R_{dA} , is

$$R_{dA} = \frac{d\sigma_{J/\psi}^{dAu}/dy}{(2 \times 197) \times d\sigma_{J/\psi}^{pp}/dy} \quad (2)$$

In the above expressions B_{ll} is the J/ψ branching ratio to di-leptons, $N_{J/\psi}$ is the measured J/ψ yield, A is the geometrical acceptance, ϵ_{rec} is the di-lepton reconstruction efficiency, ϵ_{trig} is the trigger efficiency, N_{evt} is the number of min-bias triggers sampled, σ_{MB}^{tot} is the total minimum-bias (MB) cross section, Δy is the rapidity bin width, and ϵ_{MB}^{BBC} and $\epsilon_{J/\psi}^{BBC}$ are the beam-beam trigger efficiencies for min-bias and J/ψ events respectively. The factor of 2×197 causes R_{dA} to be one if the $d+A$ cross section is just additive from $p+p$, i.e. if there are no nuclear modifications.

For $p+p$ we use the cross section for our beam-beam trigger, $\sigma_{MB}^{tot}(pp)\epsilon_{MB}^{BBC}(pp) = 23.0 \pm 2.2$ mb; and the efficiency for events with a J/ψ , $\epsilon_{J/\psi}^{BBC}(pp) = 0.79 \pm 0.02$. For

$d+Au$ collisions we use a beam-beam trigger cross section of $\sigma_{MB}^{tot}(dAu)\epsilon_{MB}^{BBC}(dAu) = 1.99 \pm 0.10$ b from our measurement [18] using photo-dissociation of the deuteron as a reference [19], which is consistent with our calculated Glauber result of 1.92 ± 0.18 b. For the J/ψ we use $\epsilon_{J/\psi}^{BBC}(dAu) = 0.94 \pm 0.02$ [20].

For $d+Au$ collisions, the centrality of the collision can be characterized by measuring the charge deposited in the beam-beam counter in the Au beam direction [20]. An approximate number of nucleon+nucleon collisions $\langle N_{coll} \rangle$ can be obtained through a Glauber calculation that relates this $\langle N_{coll} \rangle$ to the observed charge. In this case $R_{dA}(N_{coll})$ is calculated as,

$$R_{dA}(\langle N_{coll} \rangle) = \frac{N_{inv}^{dAu}(\langle N_{coll} \rangle)}{\langle N_{coll} \rangle \times N_{inv}^{pp}} \quad (3)$$

where the invariant yield N_{inv} is,

$$N_{inv}(\langle N_{coll} \rangle) = \frac{N_{J/\psi} C_{bias}(\langle N_{coll} \rangle)}{A \epsilon_{rec} \epsilon_{trig} [N_{evt}(\Delta w/w)]} \quad (4)$$

with $\langle N_{coll} \rangle$ being the average number of binary collisions for a particular $d+Au$ centrality bin and $N_{evt}(\Delta w/w)$ the number of $d+Au$ min-bias triggers sampled that lie in this fraction, Δw , of the total minimum-bias centrality range, w . This prescription is equivalent to that of Eq. 1,2 for minimum bias. For $p+p$ collisions $\Delta w/w$ is one. $C_{bias} = \epsilon_{MB}^{BBC}/\epsilon_{J/\psi}^{BBC}$ is a correction for the smaller trigger efficiency in minimum-bias events compared to those with a J/ψ . For $d+Au$, C_{bias} depends on $\langle N_{coll} \rangle$ and takes into account the effect of the underlying event multiplicity on both the trigger efficiency and the centrality measurement [20]. Its variation with centrality is up to 7% from unity.

For the electron analysis, $A \epsilon_{rec}$ and ϵ_{trig} were determined using a GEANT [21] simulation of the central arms and a trigger response software emulation [16]. ϵ_{rec} was confirmed by studying pairs identified as photon conversions in the data. The systematic uncertainty of 10.4% is dominated by run-to-run efficiencies (5%), yield extraction (5%), and the occupancy dependence of the efficiency (4.4%).

For the muon arms, $A \epsilon_{rec} \epsilon_{trig}$ was determined within each rapidity and p_T bin, using a GEANT simulation with J/ψ events generated by PYTHIA [22]. The dominant systematic uncertainties in our result are +6/-9% from the muon identifier efficiency and up to 10% (for the most central negative rapidity $d+Au$ data) from the combinatoric background.

Figure 1 (a) shows the measured $p+p$ differential cross section times branching ratio versus rapidity with a di-electron point at mid-rapidity and two di-muon points at negative and positive rapidities. A fit to a shape generated with PYTHIA is performed and, using a di-lepton

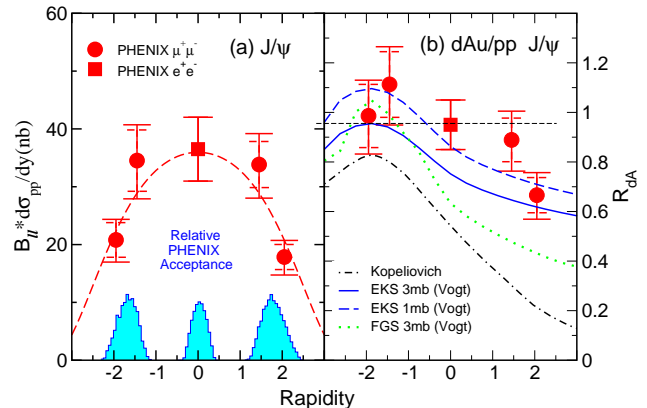


FIG. 1: (color online) (a) The 200 GeV J/ψ $p+p$ differential cross section times di-lepton branching ratio versus rapidity (10% overall normalization uncertainty is not included). (b) The minimum bias R_{dA} versus rapidity (12% overall normalization uncertainty not included). For both panels the dashed error bars represent systematic uncertainties relevant for comparing the two rapidity bins in each muon arm, while the solid error bars represent the overall uncertainties relevant for comparing points at negative, central, or positive rapidity. The curve in (a) represents a fit as described in the text while the curves in (b) are theoretical calculations [5, 24, 25] as described in the text.

branching ratio of 5.9% [23], gives a total cross section $\sigma_{pp}^{J/\psi} = 2.61 \pm 0.20(\text{fit}) \pm 0.26(\text{abs}) \mu\text{b}$. Variations in the parton distribution functions and models used to determine the shape are negligible compared to the fit errors. This result is smaller by about two sigma than our previous lower statistics result [16].

Figure 1 (b) shows the nuclear modification factor R_{dA} (Eq. 2) versus rapidity, where a value of one would correspond to no nuclear modification. While this ratio is consistent with unity at negative rapidity, it is significantly lower at the most positive rapidity where gluons are expected to be shadowed in a heavy nucleus. Theoretical predictions [5, 24, 25] that include the effects of absorption and shadowing are shown for comparison in Fig. 1 (b). The data favor a relatively modest shadowing in agreement with the parametrization of Eskola-Kolhinen-Salgado (EKS) based on a leading-twist Dokshitzer-Gribov-Lipatov-Altarelli-Parisi-evolved parametrization of nuclear deep inelastic scattering and Drell-Yan data at lower energies [3], rather than the stronger gluon shadowing of Kopeliovich [5] or Frankfurt-Guzey-Strikman (FGS) [4] based on models involving coherence for a $q\bar{q}$ dipole in the nucleus. The $c\bar{c}$ absorption cross section is not well determined by our data, but is probably nearer to 1 mb and is certainly smaller than the 4.1 ± 0.4 mb found at lower energy [26].

Lower energy $p+A$ measurements showed that J/ψ

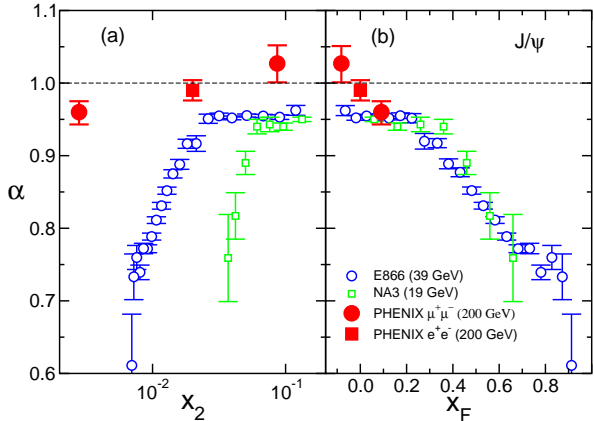


FIG. 2: (color online) α versus (a) α versus p_T compared to lower energy measurements shown for three different x_F ranges. An additional overall uncertainty of 0.02 in our α values is not shown.

suppression did not follow a universal behavior vs x_2 [27], the momentum fraction in the heavy nucleus, as would be expected if the suppression was dominated by shadowing [10]. As shown in Fig. 2 (a), our data confirm this x_2 scaling violation with the addition of a smaller x_2 point, but with our small range in x_F have little to add to the approximate x_F scaling observed in these lower energy measurements [see Fig. 2 (b)]. Here α is defined by $\sigma_{dA} = \sigma_{pp} \times (2A)^\alpha$ and $x_F = x_1 - x_2$, where x_1 is the momentum fraction of the gluon in the deuteron. This x_F scaling may be caused by energy loss of the gluon in the initial state [7], or by an energy conservation effect (“Sudakov suppression”) [28] which causes a universal suppression that increases with x_F for production of J/ψ 's and other hadrons. It is also similar to that observed for more positive rapidity hadron production in the $d + Au$ “limiting fragmentation” region [29].

Invariant cross sections versus transverse momentum, $(d^2\sigma/dydp_T)/(2\pi p_T)$, have been fit to the form $A \times (1 + (p_T/B)^2)^{-6}$ [30]. Average p_T^2 values resulting from these fits are 4.28 ± 0.31 , 3.03 ± 0.40 and 3.63 ± 0.25 GeV/c^2 for $d + Au$ collisions at negative, zero, and positive x_F , respectively; compared with 2.51 ± 0.21 and 4.31 ± 0.85 GeV/c^2 for negative/positive and zero x_F $p + p$ collisions, respectively. The observed p_T broadening is shown in Fig. 3 (a). For negative x_F it is consistent with that of the lower energy ($\sqrt{s_{NN}} = 39$ GeV) measurements from E866/NuSea [10], but may be flatter at positive x_F . At zero x_F no p_T broadening is seen within errors.

R_{dA} (Eq. 3) is shown in Fig. 3 (b) for four centrality classes and for minimum bias collisions. This classification into centrality bins for these results can only be approximate, as indicated by the overlapping histograms of N_{coll} . At positive rapidity (small x_2 , or the shadowing

region), a weak drop for more central collisions is observed, while no significant centrality dependence is seen for negative rapidity or for central rapidity. The theoretical curves on Fig. 3 (b) correspond to different amounts of density dependent shadowing and anti-shadowing [24, 25] and also include absorption. They are consistent with our data except at positive rapidity where the EKS shadowing curve is closest to our results, although slightly lower perhaps due to the amount of absorption that is included.

In summary, during the RHIC 2003 run, the PHENIX experiment measured nuclear effects on J/ψ production for $d + Au$ collisions at $\sqrt{s_{NN}} = 200$ GeV. Increasing suppression for larger rapidity (smaller x_2) and for more central collisions (higher nuclear densities sampled) both are consistent with models containing a small amount of impact-parameter dependent shadowing and with weak absorption. Theoretical calculations which include EKS shadowing seem most consistent with the data. However comparisons with other measurements at lower energies show that shadowing cannot be the dominant effect, at least not for the lower energy measurements. We also see some transverse momentum broadening which is consistent with that seen at lower energy. Higher luminosity $d + Au$ running in the future yielding higher numbers of J/ψ 's will be necessary to quantify these nuclear effects and to more clearly distinguish between various theoretical models of shadowing, absorption and other cold nuclear matter effects.

We thank the staff of the Collider-Accelerator and Physics Departments at BNL for their vital contributions. We acknowledge support from the Department of Energy and NSF (U.S.A.), MEXT and JSPS (Japan), CNPq and FAPESP (Brazil), NSFC (China), IN2P3/CNRS, CEA, and ARMINES (France), BMBF, DAAD, and AvH (Germany), OTKA (Hungary), DAE and DST (India), ISF (Israel), KRF and CHEP (Korea), RMIST, RAS, and RMAE (Russia), VR and KAW (Sweden), U.S. CRDF for the FSU, US-Hungarian NSF-OTKA-MTA, and US-Israel BSF.

* Deceased

† PHENIX Spokesperson:zajc@nevis.columbia.edu

- [1] M. Bedjidian et al. hep-ph/0311048 (2003).
- [2] T. Matsui and H. Satz, Phys. Lett. **B178**, 416 (1986).
- [3] K. J. Eskola, V. J. Kolhinen, and R. Vogt, Nucl. Phys. **A696**, 729 (2001).
- [4] L. Frankfurt, V. Guzey, and M. Strikman, Eur. Phys. J. **A5**, 293 (1999).
- [5] B. Kopeliovich, A. Tarasov, and J. Hüfner, Nucl. Phys. **A696**, 669 (2001).
- [6] L. McLerran and R. Venugopalan, Phys. Rev. D **49**, 2233 (1994).
- [7] R. Vogt, Phys. Rev. C **61**, 035203 (2000).
- [8] L. Antoniazzi et al. Phys. Rev. Lett. **70**, 383 (1993).
- [9] D. M. Alde et al., Phys. Rev. Lett. **66**, 133 (1991).

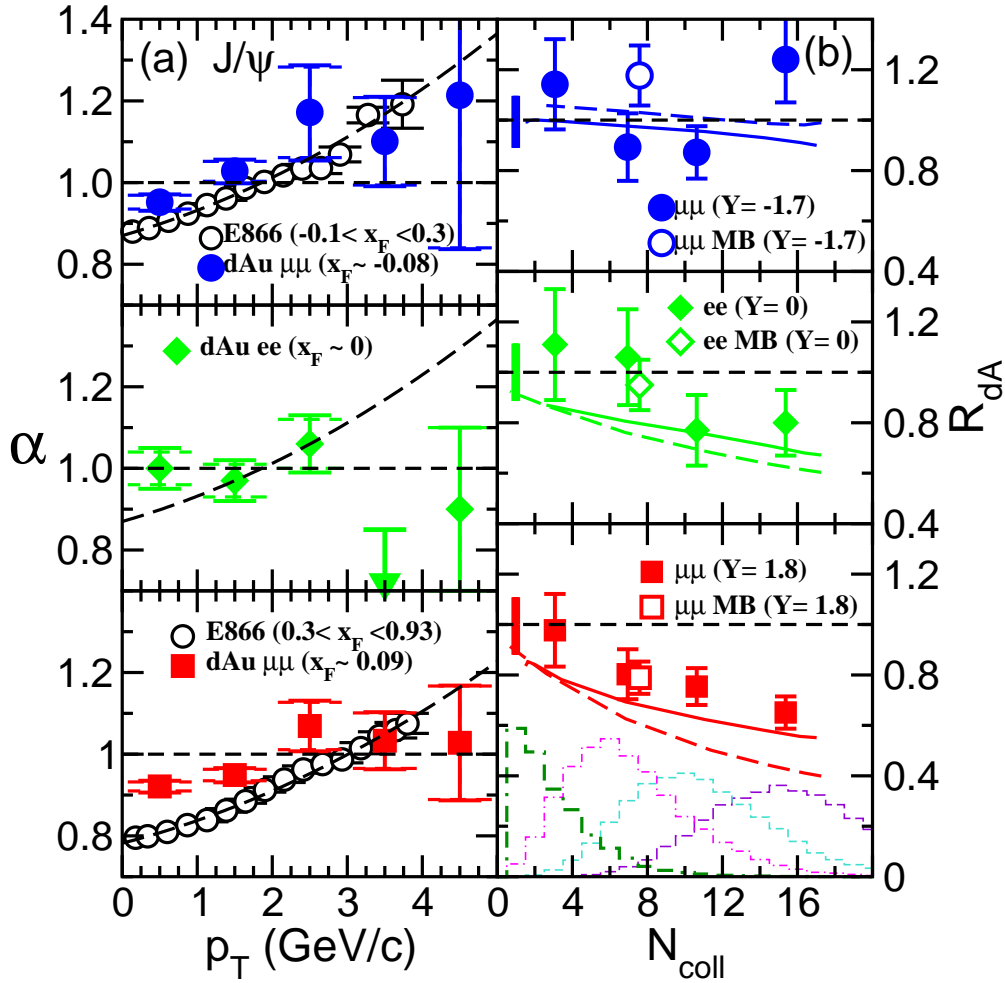


FIG. 3: (color online) (a) α versus p_T compared to lower energy measurements, shown for three different x_F ranges. The error bars have the same meaning as in Fig. 1. An additional 0.02 overall uncertainty is not shown. The dashed curves are simple fits [10] to the lower energy results. (b) Nuclear modification factor versus centrality as given by the number of nucleon+nucleon collisions shown for three different rapidity ranges, compared to theoretical calculations[24, 25] including final-state absorption and EKS (solid) or FGS (dashed) shadowing. The bars at the low end of each plot represent the systematic errors between different rapidity ranges. An additional 12% global error bar is not shown. The histograms at the bottom of the lower panel indicate the distribution of the number of collisions for each of the four centrality bins.

- [10] M. J. Leitch et al., Phys. Rev. Lett. **84**, 3256 (2000).
 [11] B. Alessandro et al., Phys. Lett. **B553**, 167 (2003).
 [12] J. Spengler J. Phys. **G30**, S871 (2004).
 [13] J. Badier et al., Z. Phys. **C20**, 101 (1983).
 [14] M. J. Leitch, Eur. Phys. J A **S19**, 129 (2004).
 [15] S. S. Adler et al., Nucl. Instrum. Meth. **A499**, 469 (2003).
 [16] S. S. Adler et al., Phys. Rev. Lett. **92**, 051802 (2004).
 [17] S. S. Adler et al., Phys. Rev. C **69**, 014901 (2004).
 [18] S. N. White, *Proceedings of the XIIIth International Workshop DIS'05, Madison, WI, 2005*, edited by W.H. Smith [AIP Conf. Proc., **792**, No. 1, 527, (2005)].
 [19] S. R. Klein and R. Vogt, Phys. Rev. C **67**, 047901 (2003).
 [20] S. S. Adler et al., Phys. Rev. Lett. **94**, 082302 (2005).
 [21] F. Carminati et al., "GEANT: Detector Description and Simulation Tool", CERN Program Library Long Writeup No. W5013, 1993 (unpublished).
 [22] T. Sjostrand et al., Comput. Phys. Commun. **135**, 238 (2001).
 [23] S. Eidelman et al., Phys. Lett. **B592**, 1 (2004).
 [24] S. R. Klein and R. Vogt, Phys. Rev. Lett. **91**, 142301 (2003).
 [25] R. Vogt, Phys. Rev. C **71**, 054902 (2005).
 [26] G. Borges, et al. hep-ex/0505065 (2004).
 [27] $x_2 = 0.5(-x_F + \sqrt{x_F^2 + 4M_{J/\psi}^2/s_{NN}})$.
 [28] B. Z. Kopeliovich, et al. hep-ph/0501260 (2005).
 [29] B. B. Back et al., Phys. Rev. Lett. **93**, 082301 (2004).
 [30] J. K. Yoh et al., Phys. Rev. Lett. **41**, 684 (1978).